Research Article

Hu Niu*, Yan Xing, Shusen Chen, Shaohua Jin, and Lijie Li

Molecular dynamics simulations of dihydroxylammonium 5,5′-bistetrazole-1,1′-diolate (TKX-50) and TKX-50-based PBXs with four energetic binders

https://doi.org/10.1515/epoly-2023-0024
received March 29, 2023; accepted May 22, 2023

Abstract: Four energetic binders, polyglycidyl nitrate (PGN), poly(3-nitratomethyl-3-methyloxetane) (PNIMMO), poly(bis(azidomethyl)oxetane) (PBAMO), and glycidyl azide polymer (GAP) were, respectively, mixed with dihydroxylammonium 5,5′-bistetrazole-1,1′-diolate (TKX-50), forming TKX-50-based polymer bonded explosives (PBXs). Interfacial forces (binding energies) under different temperatures, mechanical properties (tensile modulus, bulk modulus, shear modulus, and Poisson's ratio), and moldability of TKX-50-based PBXs were investigated by employing molecular dynamics simulation, the energy characteristics of TKX-50-based PBXs were calculated by Chapman–Jouguet (C–J) detonated theory. Results show that temperature has little effect on the binding energies, but the binding energies between every energetic binder and each surface of TKX-50 are different and the order of combined ability between four energetic binders and TKX-50 decrease as follows: PNIMMO > PBAMO > PGN > GAP. Compared with TKX-50, the addition of four energetic binders makes the rigidity of TKX-50-based PBXs decrease and the plasticity improve, the plastic ability rank is in the order of PGN > PNIMMO > PBAMO > GAP. In addition, the moldability of TKX-50-based PBXs is obviously improved, the increasing order is PGN > PNIMMO > PBAMO > GAP. Finally, the detonation performances indicate that compared with common binder, the addition of the energetic binder makes TKX-50-based PBXs have higher energy under the same condition.

Keywords: TKX-50, PBXs, molecular dynamics, energetic binder

*** Corresponding author: Hu Niu**, China Aerospace Components Engineering Center, China Academy of Space Technology, Beijing, China, e-mail: 455615961@qq.com
Yan Xing: China Aerospace Components Engineering Center, China Academy of Space Technology, Beijing, China
Shusen Chen, **Shaohua Jin**, **Lijie Li:** School of Materials Science and Engineering, Beijing Institute of Technology, Beijing, China

1 Introduction

Developing insensitive munitions (IMs) is always the major trend in the sector of propellants and explosives (1–3). Therefore, up till now, a lot of IMs have been designed and prepared through great efforts of scientific researchers (4–6). Among them, dihydroxylammonium 5,5′-bistetrazole-1,1′-diolate (TKX-50) is noticeable especially, because it is not only very insensitive but also highly energetic (7), which also breaks the traditional view that high energy must be accompanied with high sensitivity. Just for the special superiority of TKX-50, it is considered to be a promising candidate for a new generation of high energetic insensitive material and many properties including synthesis, decomposition mechanism, molecular structure, compatibility, and thermal behavior have been studied in recent years (8–12). However, as a new kind of energetic material, it is necessary to convert single explosive compound into its polymer bonded explosive (PBX) in order to promote its application, because PBXs can be widely used in military and civilian field due to their simple preparation, superior mechanics, and high safety (13–15). When preparing PBXs, even though the kinds of poly binders are always different, the addition of the most poly binders also weakens the energy level while reducing their sensitivity.

Thus, in our research, to obtain the insensitive PBXs with the minimum energy loss, four different energetic binders polyglycidyl nitrate (PGN), poly(3-nitratomethyl-3-methyloxetane) (PNIMMO), poly(bis(azidomethyl)oxetane) (PBAMO), and glycidyl azide polymer (GAP) were chosen to be mixed with TKX-50 (Scheme 1) due to their higher energy. TKX-50-based PBXs with the four energetic binders were established in the molecular model. The binding energies under different temperatures, mechanical properties (tensile modulus, bulk modulus, shear modulus, and Poisson's ratio), and moldability of TKX-50-based PBXs were studied by using molecular dynamics (MD) simulation. In addition, the detonation velocity and detonation pressure were estimated by Chapman–Jouguet (C–J) detonated theory.

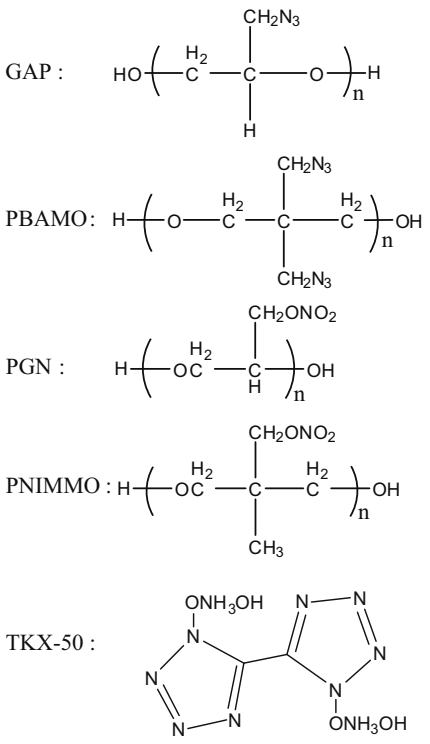

Scheme 1: Chemical structure of GAP, PBAMO, PGN, PNIMMO, and TKX-50.

Our studies are helpful for promoting the application of TKX-50 and the results are instructional and valuable for the design and preparation of TKX-50-based PBXs.

2 Methodology

2.1 Establishment of force fields

The choice of the force field is vital in the process of MD simulation, because unsuitable force field will lead to the failing of dynamics simulation or excessive error of the simulation results. TKX-50 acts as a new energetic salt, and force fields existing in Forcite Tools of Materials Studio are not suitable for simulating. Fortunately, An et al. (16) obtained the force field parameters of TKX-50 by Quantum Mechanics calculation. Therefore, with the help of the parameters obtained by An, the DREIDING force field was recompiled for the MD simulation. In the following sections, the recompiled DREIDING force field will be called DREIDING-R for short.

2.2 Checking of the force field

The crystal parameters of TKX-50 used in our work were obtained from X-ray values. The original parameters of TKX-50-unit cell were found to be a = 5.461 Å, b = 11.612 Å, c = 6.507 Å, $\alpha = \gamma = 90°$, and β = 95.391°. In order to make sure the reliability of DREIDING-R force field, geometry optimization (GO) was carried out by using DREIDING-R and the geometric parameters (cell length, cell angle, and density) obtained from simulation (Figure 1) and experiment were compared (Table 1). The results showed that the errors of all geometric parameters are within 6%, which met the conditions of simulation calculation. In addition, with the help of DREIDING-R force field, the crystallite shape was predicted by employing the method of growth morphology at morphology module and the simulated results was compared with the experimental result obtained by scanning electron microscopy (Figure 2). Just as shown in Figure 2, the simulated and experimental results are very similar and both of them indicate that TKX-50 is a flat and spindle shaped crystal, which demonstrate that the DREIDING-R force field is reliable.

The simulated results also illustrate that there are four main crystal surfaces (010), (100), (0-11), and (101) for TKX-50, and the detailed distribution is shown in Figure 3.

2.3 Construction of polymer models

For the constructions of the four energetic binders, the weight percent of the binders in PBXs were kept at about 10%. According to their structures in Scheme 1, the repeat units for GAP, PBAMO, PGN, and PNIMMO were calculated to be 8, 5, 6, and 5, respectively. Considering the four binders are all amorphous polymers, the cell amorphous models were employed to obtain their most real form according to their actual density (1.30, 1.30, 1.46, and 1.26 g·cm^{-3} for GAP, PBAMO, PGN, and PNIMMO, respectively). During the process, the length and width of all the models should be determined on the basis of the lattice parameters of the TKX-50 cells to ensure that all the binder models and TKX-50 models can be easily combined. Afterward, the four binder models were counted for 100 ps NVT MD simulation at 298 K with DREIDING-R force field, in which the thermostat method is “Anderson,” and the time step is 0.5 fs. The equilibrium structures of binders can be obtained at the end of MD simulation.

2.4 Construction of TKX-50 models

Since the properties of each crystal surface for TKX-50 are different, it is essential to cut the four main crystal surfaces (010), (100), (0-11), and (101) out from TKX-50 and construct their super cells. The cutting method can be found in the

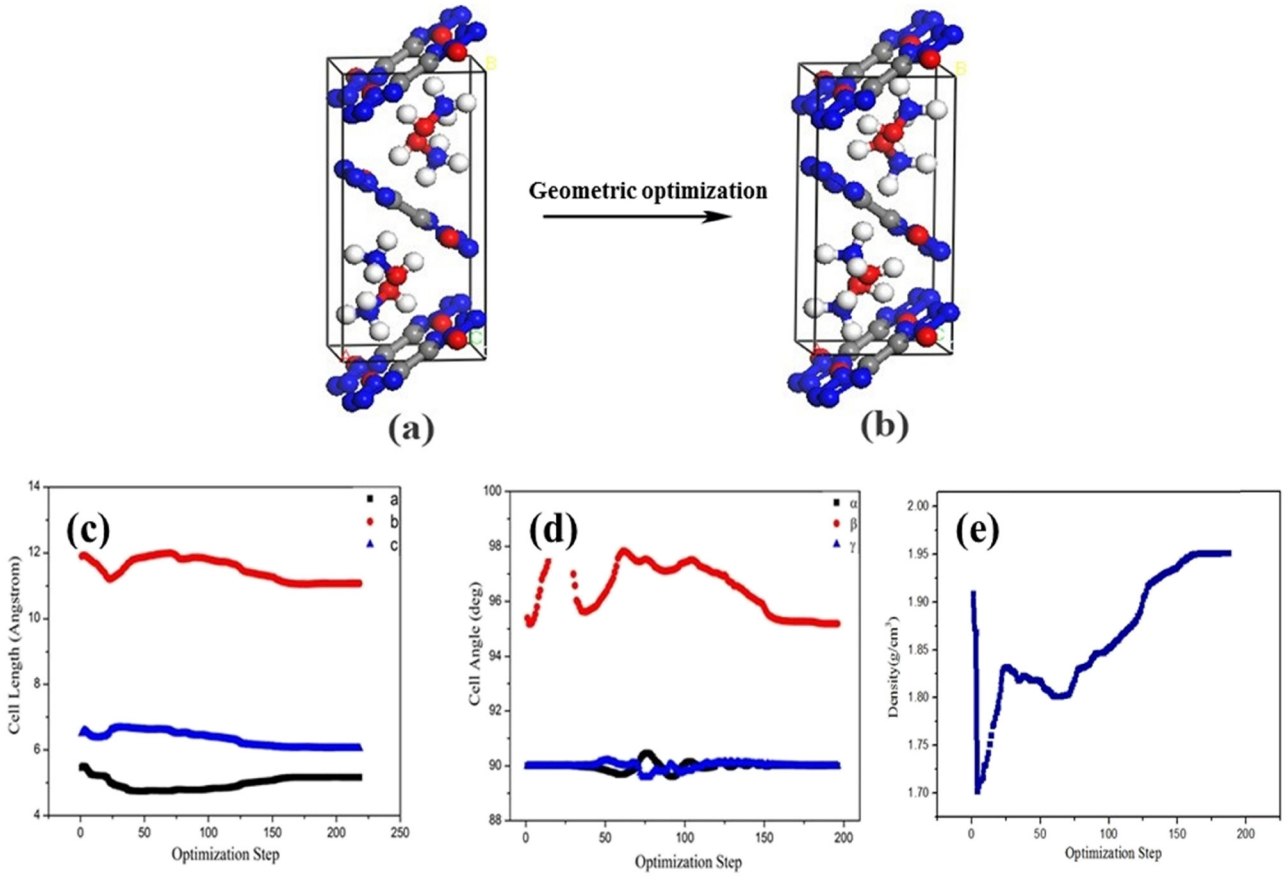

Figure 1: The simulation results of geometric parameters of TKX-50: (a) initial crystal cell structure of TXK-50, (b) crystal cell structure of geometry optimized TKX-50, (c) the variation in cell length with optimization step, (d) the variation in cell angle with optimization step, and (e) the variation in density with optimization step.

Table 1: Comparison of simulated and experimental geometric parameters of TKX-50 cell

Geometric parameters	*a*	*b*	*c*	*α*	*γ*	*β*	*D*
Experiment	5.461	11.612	6.507	90°	90°	95.391°	1.877
Simulation	5.266	11.282	6.149	90°	90°	95.189°	1.952
Error (%)	3.57	2.84	5.5	0	0	0.21	4.0

a/*b*/*c* represent the cell length, *α*/*γ*/*β* represent the cell angle, *D* represents density.

"Build" toolbar in Material Studio 6.0. To make sure the ratios of energetic binder and explosive remain consistent, the number of TKX-50 molecules in each super cell was calculated to be 40. With the help of DREIDING-R, a brief MD was carried out, by which, we can obtain the initial density of each super cell. Then, the values in the direction c were modified to get the super cells with real density (1.877 g·cm^{-3}) [7]. Finally, the four super cells were optimized by using GO and treated as the single TKX-50 models (Figure 5a) for the subsequent MD simulation.

2.5 Construction of TKX-50/binders models

Combining equilibrium structures of binders and the four super cells (010), (100), (0-11), and (101) of TKX-50 together by using "Build Layers" toolbar. To obtain the models for calculating the binding energies (E_{binding}) between TKX-50 and binders, the space in the direction c of TKX-50/binders should be expanded by 50 Å to ensure that the binders will not be affected by the TKX-50 in the upper space. Then, TKX-50/binders were made a brief GO (about 1,000 steps) to obtain the initial models (Figure 4), which can be used to carry out MD to obtain equilibrium models. Finally, the equilibrium models can be employed to calculate the E_{binding} values between TKX-50 and each energetic binder.

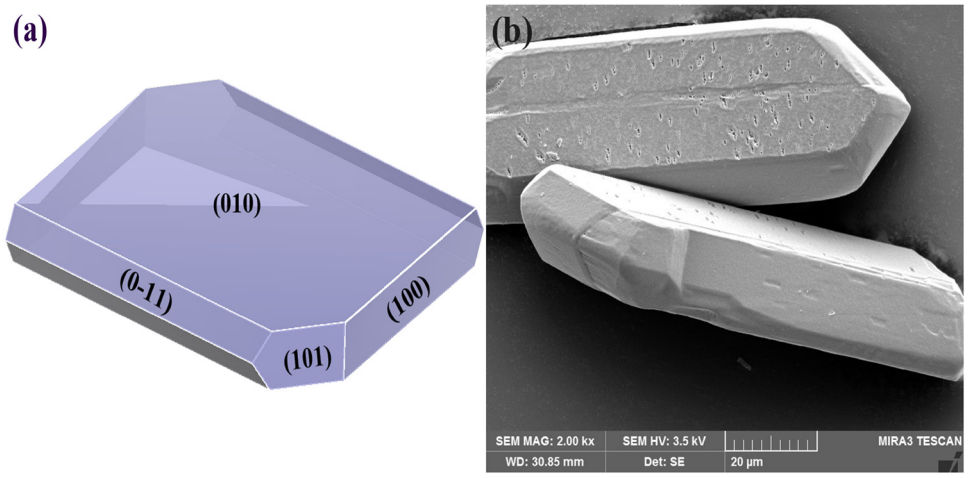

Figure 2: The simulated (a) and experimental (b) results of crystal morphology for TKX-50.

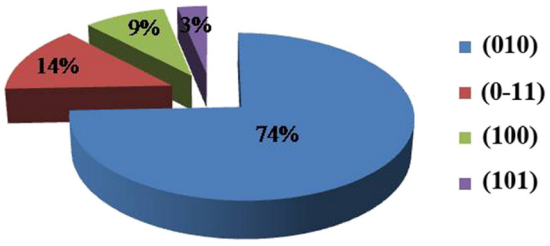

Figure 3: The distribution map of different crystal surfaces for TKX-50.

However, in order to analysis mechanical properties of TKX-50/binder by DREIDING-R force field, the combined models should be compressed in direction *c* to make their density close to the theoretical values (TKX-50/PNIMMO, 1.815 g·cm^{-3}; TKX-50/PBAMO, 1.820 g cm^{-3}; TKX-50/PGN, 1.835 g·cm^{-3}; TKX-50/GAP, 1.819 g·cm^{-3}). Then, TKX-50/binders models were made a brief GO (about 1,000 steps) to obtain the initial models (Figure 5b) for carrying out MD simulation. Finally, the equilibrium models of TKX-50/binder can be obtained and used to analysis the mechanical properties and moldabilities.

In all the MD simulations above, the single TKX-50 and TKX-50/binders were treated as isothermal-isochoric (*NVT*) ensemble. The initial velocities are assigned at random from a Maxwell–Boltzmann distribution. During the simulation process, a non-bond (electrostatic and van der Waals) was obtained by the Ewald and atom-based method. "Anderson" was chosen as the thermostat, and the temperatures were set as 298 K for simulations of mechanical properties and 298, 308, 318, 328, 338, and 348 K for simulations of binding energies. The time step was 1 fs and the

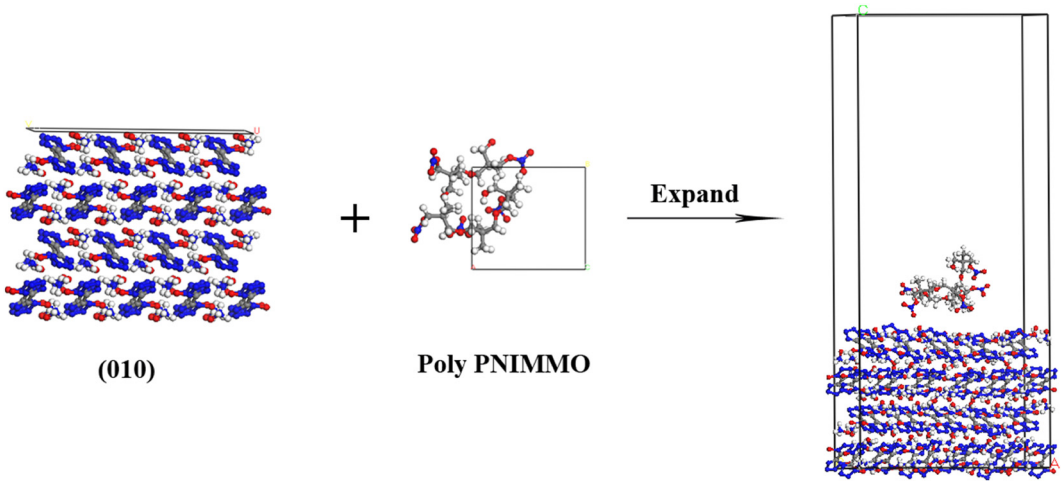

Figure 4: The initial model of TKX-50-based PBX ((010)/PNIMMO).

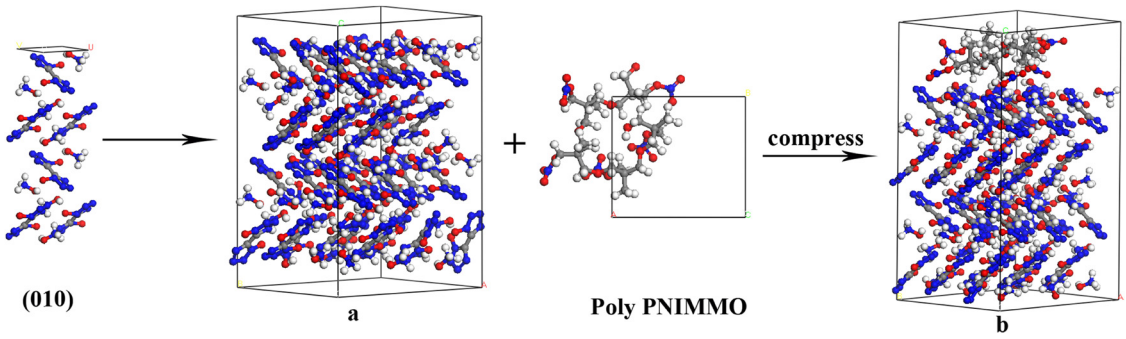

Figure 5: The initial models of TKX-50 (a) and TKX-50-based PBX (b) for analyzing the mechanical properties ((010)/PNIMMO).

total simulation step number was 200,000. The frame was output every 50 steps, so 4,000 frames would be saved and put out. Five frames with the minimum energy were chosen as equilibrium models to analyze their binding energies and mechanical properties.

3 Results and discussion

3.1 Binding energies

The value of binding energy ($E_{binding}$) can directly show the abilities of the four energetic binders coated TKX-50 and it is defined as the negative value of the interaction energy (E_{inter}), that is, $E_{binding} = -E_{inter}$. The molecular interaction energy can be estimated by calculating the single point total energy of each component in the equilibrium models. In terms of our research works, the values of E_{inter} between the four energetic binders and TKX-50 can be described as the follows:

$$E_{inter} = E_{total} - (E_{TKX\text{-}50} + E_{binder}) \quad (1)$$

where E_{total} is the average total energy of PBX, $E_{TKX\text{-}50}$ and E_{binder} are the average single point energy of TKX-50 and the four energetic binders, respectively.

Only when the model reaches equilibrium, can the $E_{binding}$ be analyzed. We can determine whether a model is in an equilibrium stage by observing the fluctuations of temperature and energy. A model is usually considered to be a balance when its fluctuation ranges of temperature and energy are less than 10% (17–19). Take TKX-50(010)/PNIMMO as an example. Figure 6 presents its fluctuation curves of temperature (Figure 6a) and energy (Figure 6b) obtained from the last 100 ps molecular simulation.

From Figure 6, it can be seen that the fluctuating ranges are less than 3% for both temperature and energy. The results demonstrate that our model has reached an equilibrium stage. The other 15 TKX-50/binders can obtain their equilibrium models using the same method. The equilibrium models of (010) crystalline surface with the four energetic binders are shown in Figure 6 as an example. It can be seen that all the binders are closer to the crystal surface compared with their initial models and this may be

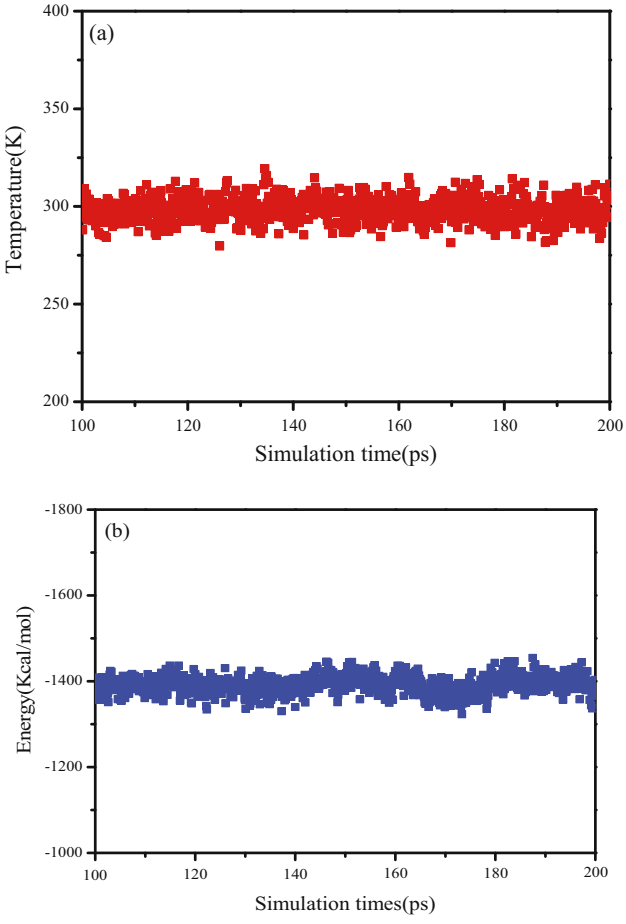

Figure 6: Fluctuation curves of (a) temperature and (b) energy of (010)/PNIMMO.

Table 2: Average energies (kJ·mol^{-1}) of each component in PBXs and the average binding energies (kJ·mol^{-1}) between different crystal surface and the four energetic binders at 298 K of equilibrium models

Facet	Binders	E_{total}	E_{facet}	E_{binder}	$E_{binding}$
(010)	PNIMMO	−6,160.32	−7,583.29	1,510.79	87.82
	PGN	−5,938.52	−7,453.53	1,565.19	50.18
	PBAMO	−7,072.65	−7,733.04	728.19	67.8
	GAP	−7,219.13	−7,803.36	611.01	26.78
(0–11)	PNIMMO	−6,293.81	−7,800.46	1,581.93	75.28
	PGN	−5,726.13	−7,199.31	1,544.27	71.09
	PBAMO	−7,177.58	−7,887.36	744.93	35.15
	GAP	−7,021.94	−7,550.09	556.61	28.46
(100)	PNIMMO	−5,389.42	−6,875.15	1,552.64	66.91
	PGN	−5,710.35	−7,505.76	1,858.14	62.73
	PBAMO	−6,892.82	−7,502.16	657.05	47.71
	GAP	−6,937.63	−7,826.52	903.96	15.07
(101)	PNIMMO	−5,592.17	−7,098.81	1,556.82	50.18
	PGN	−5,571.79	−7,019.85	1,510.79	62.73
	PBAMO	−6,853.29	−7,572.28	749.12	30.13
	GAP	−6,973.14	−7,634.37	686.34	25.11

caused by the attraction between the binder and TKX-50 crystals. In Table 2, the average energies of PBXs (E_{total}), energetic binders (E_{binder}) and TKX-50 (E_{TKX-50}) of equilibrium models (Figure 7) are presented, by which, the average binding energies ($E_{binding}$) of equilibrium models were calculated.

The data in Table 2 clearly show that the values of binding energies between diverse binders and the same crystal surface of TKX-50 are very different, these results may be caused by the different functional groups of binders. Generally, PNIMMO presented the stronger binding force with every crystal surface than the other three energetic binders, while the binding energies between GAP and each crystal surface of TKX-50 are the smallest among the four binders. For surface (010), its binding energy with PBAMO is larger than that of PGN; however, for the other three crystal surfaces, the values of $E_{binding}$ between PGN and the surfaces are higher than those of PBAMO. This illustrates that values of $E_{binding}$ between the same binder and different crystalline surfaces are also different, which may be caused by the different atoms on the surface of each crystalline surface of TKX-50. Furthermore, it can be found that (010) surface of TKX-50 has larger binding energies with the four energetic binders compared with the other three crystalline surfaces. Just as described in Figure 3, (010) is the largest surface among the crystalline surfaces of TKX-50. Therefore, we can conclude that when using the four energetic binders to prepare TKX-50-based PBXs, binders mainly covered on the surface of (010) and the coating effect of (010)/binder is the best.

In order to present the weighted binding effect between TKX-50 crystal and the four energetic binders, average values of $E_{binding}$ were calculated according to the area percentage of each crystalline surface. The results are listed in Table 3, which revealed that the binding abilities of TKX-50 with the four energetic binders were quite different, they decreased as follows: PNIMMO > PBAMO > PGN > GAP. This may be caused by different intermolecular van der Waals force and hydrogen bond between binders and TKX-50. As we know, the greater the electronegativity, the stronger the hydrogen bond force formed. The electronegativity of $-ONO_2$ is 3.53 and $-N_3$ is 3.04; therefore, the hydrogen bond of $-ONO_2$ and −OH is stronger than $-N_3$ and −OH. So, the binding ability of PGN with TKX-50 is better than

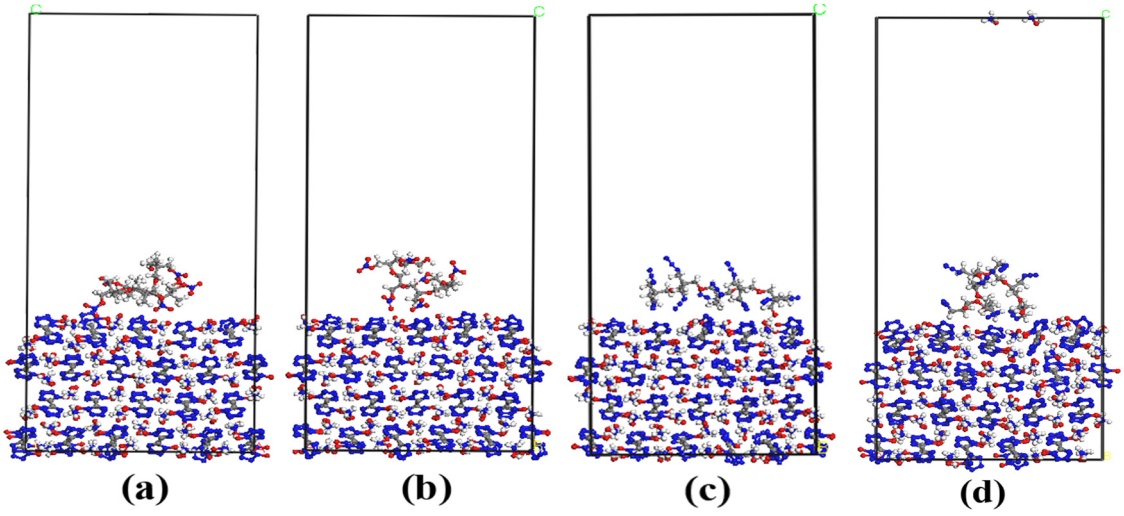

Figure 7: Equilibrium structures of (010)/binders for calculating the binding energies: (a) PNIMMO, (b) PGN, (c) PBAMO, and (d) GAP.

Table 3: Average values of $E_{binding}$ (kJ·mol^{-1}) for TKX-50-based PBXs with the four energetic binders

System	TKX-50/PGN	TKX-50/PNIMMO	TKX-50/PBAMO	TKX-50/GAP
$E_{binding}$	54.52	83.04	60.37	25.91

GAP with TKX-50, the binding ability of PNIMMO with TKX-50 is better than PBAMO with TKX-50. In addition, the van der Waals force of PBAMO is greater than PGN. Therefore, when considering hydrogen bonding and van der Waals forces comprehensively, the result of interaction between different adhesives and TKX-50 is PNIMMO > PBAMO > PGN > GAP.

In order to verify the simulation result, the preparation of TKX-50-PBX was carried out by using PNIMMO, PBAMO, and TKX-50. The experiment results (Figure 8) show that TKX-50/PNIMMO is granular, indicating that PNIMMO sticks TKX-50 together and TKX-50/PBAMO is powder, indicating that PBAMO fails to stick TKX-50 together, which means that only TKX-50-PNIMMO bonded explosive can be prepared successfully, and this is consistent with our calculation result.

As we all know, the temperature during the preparations of PBXs is always higher than the room temperature. So, for more reference value, the effects of different temperatures (298, 308, 318, 328, 338, and 348 K) on binding energies of TKX-50/binders were studied. The simulated results are listed in Table 4 and shown in Figure 9.

As shown in Figure 9, the average binding energies are almost constant for TKX-50/PNIMMO, TKX-50/PBAMO, and TKX-50/GAP systems, which means that temperature has weak effect on the binding energies of the three systems. However, for TKX-50/PGN, it can be found that the value of

Table 4: Average binding energies (kJ·mol^{-1}) of TKX-50 with the four energetic binders at different temperatures

Systems	298 K	308 K	318 K	328 K	338 K	348 K
(010)/PNIMMO	87.82	83.64	83.64	96.19	92.00	83.64
(0-11)/PNIMMO	75.28	83.64	79.46	79.46	92.00	66.91
(100)/PNIMMO	66.91	79.46	75.28	83.64	75.28	87.82
(101)/PNIMMO	50.18	62.73	62.73	58.55	66.91	71.09
TKX-50/PNIMMO	83.04	82.58	81.64	91.58	89.69	81.33
(010)/PGN	50.18	75.28	16.73	50.18	66.91	46.00
(0-11)/PGN	71.09	54.37	75.28	58.55	71.09	46.00
(100)/PGN	62.73	46.00	54.37	50.18	50.18	50.18
(101)/PGN	62.73	71.09	71.09	62.73	62.73	79.46
TKX-50/PGN	54.52	69.70	29.74	51.71	65.84	47.45
(010)/PBAMO	67.80	65.29	70.31	72.82	62.78	70.31
(0-11)/PBAMO	35.15	35.15	37.67	40.18	32.64	40.18
(100)/PBAMO	47.71	45.20	45.20	42.69	45.20	47.71
(101)/PBAMO	30.13	32.64	37.67	35.15	35.15	32.64
TKX-50/PBAMO	60.37	58.36	62.60	64.50	56.24	63.00
(010)/GAP	26.78	23.44	30.13	18.41	25.11	26.78
(0-11)/GAP	28.46	25.11	30.13	21.76	28.46	30.13
(100)/GAP	15.07	18.41	10.04	15.07	18.41	16.74
(101)/GAP	25.11	16.74	23.44	20.09	21.76	26.78
TKX-50/GAP	25.91	23.00	28.12	18.62	24.85	26.34

$E_{binding}$ is the smallest when the temperature is 318 K, which is mainly caused when a sharp decline of $E_{binding}$ occurs in (010)/PGN ensemble at this temperature. Hence, it indicates that we should avoid preparing TKX-50-based PBX at 318 K when using PGN as a binder.

3.2 Mechanical properties

The mechanical properties are critical characteristics of PBX, and they can be measured by using PBX grains. In

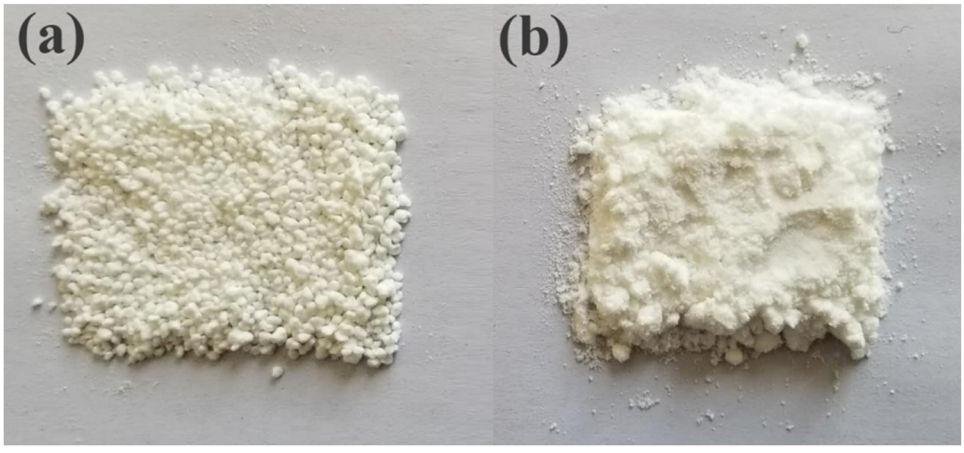

Figure 8: (a) TKX-50/PNIMMO- and (b) TKX-50/PBAMO-bonded explosives.

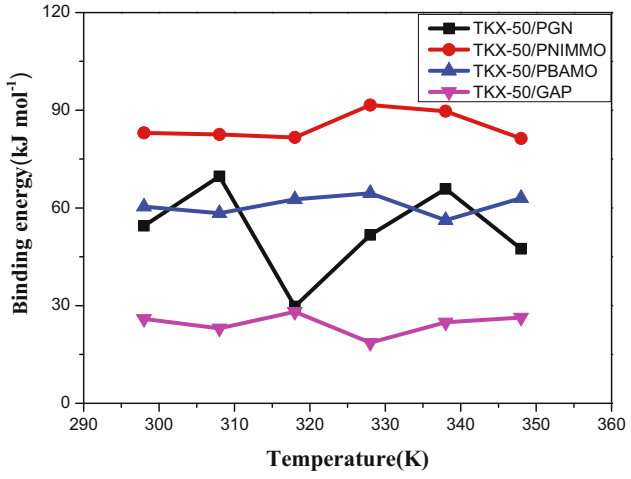

Figure 9: The trend of variations in binding energy of TKX-50/binders with the change in temperature.

fact, the mechanical properties of PBX are presented through the binders, because the explosives in PBX are brittle materials, while binders are ductile materials, and it is the binders that can bear large deformation and transfer stress. For the PBXs, which have not been obtained via experimental method, we can predict their relationships between stress and strain by means of the generalized Hook's law (20) as given in Eq. 2.

$$\begin{bmatrix}\sigma_x\\ \sigma_y\\ \sigma_z\\ \tau_{yz}\\ \tau_{xz}\\ \tau_{xy}\end{bmatrix} = \begin{bmatrix}C_{11} & C_{12} & C_{13} & C_{14} & C_{15} & C_{16}\\ C_{21} & C_{22} & C_{23} & C_{24} & C_{25} & C_{26}\\ C_{31} & C_{32} & C_{33} & C_{34} & C_{35} & C_{36}\\ C_{41} & C_{42} & C_{43} & C_{44} & C_{45} & C_{46}\\ C_{51} & C_{52} & C_{53} & C_{54} & C_{55} & C_{56}\\ C_{61} & C_{62} & C_{63} & C_{64} & C_{65} & C_{66}\end{bmatrix}\begin{bmatrix}\varepsilon_x\\ \varepsilon_y\\ \varepsilon_z\\ \gamma_{yz}\\ \gamma_{xz}\\ \gamma_{xy}\end{bmatrix} \quad (2)$$

where σ is the stress tensor, C is the elastic coefficient, and ε represents the strain tensor. Due to the existence of the strain energy, the matrix is symmetric, which means $C_{ij} = C_{ji}$. Therefore, 21 coefficients should be solved to illustrate the relationship between stress and strain for materials.

The stress tensor can be calculated by using the virial expression (21) as follows:

$$\sigma = -(1/V_o)\left[\sum_{i=1}^{N} m_i(v_i v_i^T) + (\sum_{i<j} r_{ij} f_{ij}^T)\right] \quad (3)$$

where V_o is the initial volume, i is the particle i in system, m and v are the mass and velocity, respectively, f and r represent the force and distance between the particles.

For a periodic cell, the strain tensor can be described as Eq. 4.

$$\varepsilon = (1/2)[(h_o^T)^{-1} G h_o^{-1} - 1] \quad (4)$$

where h_o is the corresponding matrix formed from the original cell vectors a_o, b_o, and c_o, h is the matrix of deformed cell vectors a, b, and c, T denotes the matrix transpose, and G is the metric tensor $h^T h$.

According to statistics, a heteromorphy consisting of micro-crystals with random orientation can be considered isotropic, the compliances in terms of single crystal compliances averaged over all orientations can be calculated by Reuss method (22). The effective bulk module (K) and shear (G) can be expressed by Eqs. 5 and 6, respectively, as follows:

$$K_R = [3(a + 2b)]^{-1} \quad (5)$$

$$G_R = \frac{5}{(4a - 4b + 3c)} \quad (6)$$

where $a = \frac{1}{3}(S_{11} + S_{22} + S_{33})$, $b = \frac{1}{3}(S_{12} + S_{23} + S_{31})$, and $c = \frac{1}{3}(S_{44} + S_{55} + S_{66})$, R represents the Reuss average, compliance matrix S is the inverse of elastic coefficient matrix C, $S = C^{-1}$. Based on the obtained K and G, the tensile module, and Poisson's ratio (m) can be calculated as follows:

$$E = 2G(1 + u) = 3K(1 - 2u) \quad (7)$$

Just as $E_{binding}$, the discussions of isotropic mechanical properties (tensile module E, bulk module K, shear module G, and Poisson's ratio μ) also need to be based on the equilibrium models. Using the same discrimination method as previously mentioned, the equilibrium models of (010)/binders for calculating their mechanical properties are obtained in Figure 10 and other 12 equilibrium models can be obtained in the same way.

According to the equilibrium models of TKX-50 and TKX-50/binders, their mechanical properties (tensile module E, bulk module K, shear module G, and Poisson's ratio μ) were calculated by executing "Mechanical Property" task in Forcite module. The detailed data are listed in Table 5.

E, K, and G can be used to determine the stiffness of materials, the greater the values, the stronger the rigidity. u is usually employed to evaluate the plasticity of materials. Just as shown in Table 5, all the values (E, K, and G) of PBXs are lower than those of single TKX-50, which indicate that the addition of binders makes the rigidity to decrease and the elasticity of PBXs to increase. In addition, comparing with single TKX-50, the values of u for PBXs become larger and this means that the plasticity of PBXs is improved. Take facet (010) and tensile module as examples, the E's value 17.86 GPa for single TKX-50 indicates the strong rigidity to resist deformation, while the values are 10.55, 8.67, 5.93, and 14.01 GPa, respectively, when tiny amounts of binders are added on (010) surface. Clearly, the mechanical properties of TKX-50/binders are related to the type of binder and the decreases in E meaning that the elasticity of PBXs are greatly enhanced. Similar results for other facets (0-11), (100), and (101) can be concluded from Table 5.

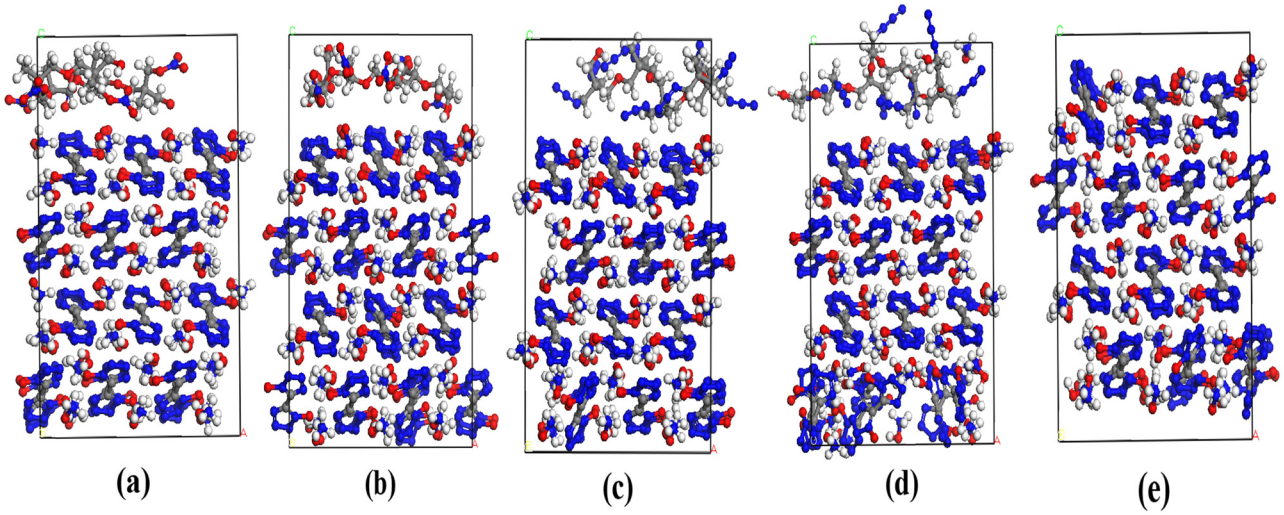

Figure 10: Equilibrium structures of (010)/binders and (010) surface for calculating the mechanical properties: (a) PNIMMO, (b) PGN, (c) PBAMO, (d) GAP, (e) (010).

Table 5: Mechanical properties of TKX-50 and TKX-50-based PBXs

Facet	System	*K* (GPa)	*G* (GPa)	*E* (GPa)	*u*
(010)	TKX-50	10.68	7.31	17.86	0.22
	TKX-50/PBAMO	9.51	4.01	10.55	0.32
	TKX-50/PNIMMO	9.15	3.23	8.67	0.34
	TKX-50/PGN	9.11	2.13	5.93	0.39
	TKX-50/GAP	10.01	5.53	14.01	0.27
(0-11)	TKX-50	11.09	6.26	15.81	0.26
	TKX-50/PBAMO	9.86	3.98	10.52	0.32
	TKX-50/PNIMMO	8.87	3.31	8.83	0.33
	TKX-50/PGN	9.13	2.56	7.02	0.37
	TKX-50/GAP	9.28	5.17	13.08	0.27
(100)	TKX-50	13.77	7.12	18.22	0.28
	TKX-50/PBAMO	10.83	4.79	12.52	0.31
	TKX-50/PNIMMO	10.22	2.99	8.17	0.37
	TKX-50/PGN	10.16	2.74	7.54	0.38
	TKX-50/GAP	11.46	4.68	12.36	0.32
(101)	TKX-50	12.36	6.81	17.26	0.27
	TKX-50/PBAMO	9.93	4.16	10.95	0.32
	TKX-50/PNIMMO	10.06	3.23	8.75	0.35
	TKX-50/PGN	10.25	3.37	9.11	0.35
	TKX-50/GAP	10.91	4.25	11.28	0.33

Meanwhile, it can be found that when the same polymer binder is added on the different crystalline surfaces, the mechanical properties results are usually different. For instance, the value of *E* of TKX-50/PBAMO (010) is 10.55 GPa, while that of TKX-50/PBAMO (100) is 12.52 GPa. In short, the simulation results indicate that compared with single TKX-50, the additions of the four energetic binders improve the mechanical properties of TKX-50-based PBXs, which are matched with that of other explosions-based PBXs (23,24).

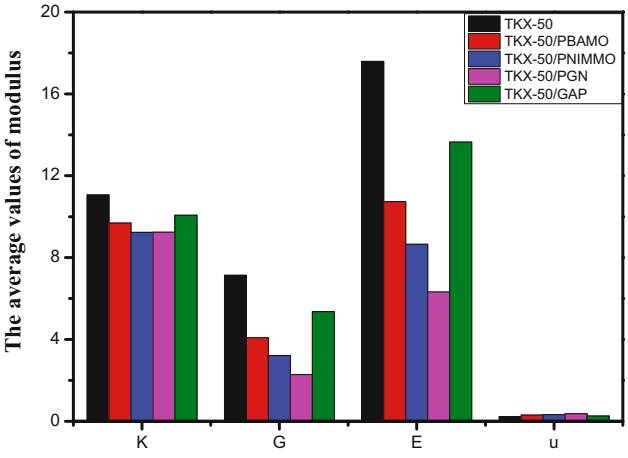

Figure 11: Mechanical properties of single TKX-50 and TKX-50-based PBXs.

Furthermore, to investigate the four binders' abilities to improve the mechanical properties of TKX-50-based PBXs, average values of *E*, *K*, G, and *u* were calculated according to the area percentage of each crystalline surface, the simulation results are shown in Figure 11, from which it can be concluded that PGN can strengthen the plasticity of TKX-50-based PBXs more significantly than the other three binders and the results are arranged in order: PGN > PNIMMO > PBAMO > GAP.

3.3 Moldability of PBXs

As mentioned above, the modulus *G* and *K* can describe the mechanical properties of materials, the two moduli

Table 6: *K/G* values of single TKX-50 and TKX-50/binders

System	*K/G*			
	(010)	(0-11)	(100)	(101)
TKX-50	1.46	1.77	1.93	1.81
TKX-50/PBAMO	2.37	2.48	2.26	2.39
TKX-50/PNIMMO	2.83	2.68	3.42	3.11
TKX-50/PGN	4.28	3.57	3.71	3.04
TKX-50/GAP	1.81	1.79	2.45	2.57

represent two mechanical behaviors: simple shear and compression. The typical feature of shear is that during the shear process, the shape of the material is the unique variable and the volume can be kept constant. However, for compression process, the volume of the material is the main variable. According to Eq. 7, when u is 0.5, then

$$G = \frac{E}{2(1+u)} = \frac{E}{3} \tag{8}$$

$$K = \frac{E}{3(1-2u)} = \infty \tag{9}$$

Eqs. 8 and 9 illustrate that when u = 0.5, the value of K/G is very large and the shape of the material can be changed much more easily than the volume, such as rubber. Therefore, the value of K/G can be employed to evaluate the moldabilities of PBXs (25).

The values of *K/G* for single TKX-50 and TKX-50/binders are shown in Table 6. Generally speaking, the great value of *K/G* means good moldability (26). Therefore, it can be concluded that (100) surface has excellent moldability for both single TKX-50 and TKX-50/binders. In addition, it can be found that due to the addition of binders, the moldabilities of TKX-50/binders are better than that of single TKX-50.

In order to know about which binder can improve the moldability of TKX-50/binders to the greatest extent, the weighted average values of *K/G* for single TKX-50 and TKX-50/binders were obtained, the calculation results are shown in Table 7. The values of *K/G* indicate that the moldability of TKX-50/PGN is better than that of TKX-50/other binders and it can be ranked in order of PGN > PNIMMO > PBAMO > GAP.

Table 7: Weighted average values of *K/G* for single TKX-50 and TKX-50/binders

System	TKX-50	TKX-50/PGN	TKX-50/PNIMMO	TKX-50/PBAMO	TKX-50/GAP
K/G	1.56	4.09	2.87	2.38	1.89

3.4 Detonation properties

For explosives, the detonation velocity (*D*) and the detonation pressure (*P*) are usually used to evaluate its basic performance. Due to the addition of energetic binders in our simulation systems, the detonation properties should be different from the systems, in which the non-energetic binders are added. To make a comparison, Dobratz method (27) is used to calculate the detonation velocity of the mixture explosive and the related equations are defined as follows:

$$D = \sum \varepsilon_i v_i \tag{10}$$

$$\varepsilon_i = \frac{m_i/\rho_i}{\sum m_i/\rho_i} \tag{11}$$

where ε_i is the volume friction of the i-th component, v_i refers to the detonation velocity (m·s^{-1}) of the i-th component, m_i is the weight (g) of the i-th component, and ρ_i presents the theoretical density (g·cm^{-3}) of the i-th component.

According to the C–J detonation theory (28) and Eq. 10, the detonation pressure can be expressed as follows:

$$P = \frac{1}{4}\rho D^2 \times 10^{-6} \tag{12}$$

Just as shown in Table 8, the differences of detonation properties for different PBXs are very small, this is because the detonation properties of PBXs are mainly determined by the single explosive in PBXs and the amounts of binders in PBXs are very small. In addition, as the energy of TKX-50 is much higher than that of binders, more binders are added, the worse the detonation properties of PBXs. Furthermore, it can be found that the detonation properties of TKX-50/binder systems in this work are better than the systems reported in our previous work (29) under the same condition, which is mainly because the energetic binders have higher energy than that of common binders. Hence, to make sure PBXs have advance detonation properties, binders which have high energies should be chosen when designing PBXs. In addition, the percentages of binders should be as small as possible under the premise that explosives can be completely coated.

Table 8: Detonation properties of TKX-50/binders with different *W*% of binders

	W% of binder	TKX-50/PGN	TKX-50/PNIMMO	TKX-50/PBAMO	TKX-50/GAP
D (m·s^{-1})	3	9,102.3	9,088.7	9,093.3	9,084.2
	10	8,904.6	8,862.2	8,875.8	8,848.3
P (GPa)	3	38.6	38.3	38.5	38.2
	10	36.3	35.6	35.8	35.5

4 Conclusion

In the work, TKX-50 and four energetic binders are employed to build models of TKX-50-based PBXs. The binding energies, mechanical properties, moldability, and detonation properties of single TKX-50 and TKX-50-based PBXs are studies via molecular simulations. The results can be summarized as follows:

1. The binding energies between every energetic binder and each surface of TKX-50 are different and the order of combined ability between four energetic binders and TKX-50 decrease as follows: PNIMMO > PBAMO > PGN > GAP. In addition, the simulation results also indicate that the temperature has little effect on the binding energies between TKX-50 and the four energetic binders.
2. The influences of the four energetic binders on the mechanical properties and moldability of different crystalline surfaces of TKX-50 are different. But all in all, the additions of the binders improve the mechanical properties and moldability of single TKX-50 and the increasing order is PGN > PNIMMO > PBAMO > GAP.
3. Since the percentages of the four energetic binders in our simulation systems are the same and small, the detonation properties for different PBXs in the work are similar. However, compared with common binders, the additions of the energetic binders improve the detonation properties significantly.

Taking the overall performances of the four energetic binders into account, PNIMMO is regarded to be a suitable binder for preparing TKX-50-based PBX due to the high binding energy, the advance mechanical properties, moldability, and detonation properties of TKX-50/PNIMMO. Therefore, PNIMMO should be given precedence as a binder when preparing TKX-50-based PBX.

Funding information: We acknowledge the financial support from Qian Xuesen Youth Innovation Fund of China Aerospace Science and Technology.

Author contributions: Hu Niu and Yan Xing wrote the main manuscript; Shusen Chen and Shaohua Jin prepared all the figures; Lijie Li prepared all the tables.

Conflict of interest: The authors state no conflict of interest.

References

(1) Li XH, Zhang C, Ju XH. Theoretical screening of bistriazole-derived energetic salts with high energetic properties and low sensitivity. RSC Adv. 2019;9:26442–9. doi: 10.1039/C9RA05141D.

(2) Zhang Q, Zhang J, Qi X, Shreeve JM. Molecular design and property prediction of high density polynitro[3.3.3]-propellane-derivatized frameworks as potential high explosives. J Phys Chem A. 2014;118:10857–65. doi: 10.1021/jp509549q.

(3) Abraham BM. High pressure structural behaviour of 5,5′-bitetrazole-1,1′-diolate based energetic materials: A comparative study from first principles calculations. RSC Adv. 2020;10:24867–76. doi: 10.1039/D0RA04782A.

(4) Zhu Q, Xiao C, Li S, Guan L. Bioinspired fabrication of insensitive HMX particles with polydopamine coating. Prop Explos Pyrotech. 2016;41:1092–7. doi: 10.1002/prep.201600021.

(5) Olivares CI, Sierra-Alvarez R, Abrell L. Zebrafish embryo toxicity of anaerobic biotransformation products from the insensitive munitions compound 2,4-dinitroanisole. Environ Toxicol Chem. 2016;35:2774–81. doi: 10.1002/etc.3446.

(6) Sahin H, Narin B, Kurtulus DF. Development of a design methodology against fast cook-off threat for insensitive munitions. Prop Explos Pyrotech. 2016;41:580–7. doi: 10.1002/prep.201500333.

(7) Fischer N, Fischer D, Klapotke TM, Piercey DG, Stierstorfer J. Pushing the limits of energetic materials - The synthesis and characterization of dihydroxylammonium 5,5′-bistetrazole-1,1′- diolate. J Mater Chem. 2012;22:20418–22. doi: 10.1039/C2JM33646D.

(8) Niu H, Chen SS, Jin SH, Shu QH, Li LJ, Shang FQ. Dissolution properties of dihydroxylammonium 5,5-bistetrazole-1,1-diolate and disodium 5,5-bistetrazole-1,1-diolate in water. J Energ Mater. 2016;34:416–25. doi: 10.1080/07370652.2015.1114048.

(9) Niu H, Chen SS, Jin SH, Li LJ, Jing BC, Jiang ZM, et al. Thermolysis, nonisothermal decomposition kinetics, calculated detonation velocity and safety assessment of dihydroxylammonium 5,5′-bistetrazole-1,1′-diolate. J Therm Anal Calor. 2016;126:473–80. doi: 10.1007/s10973-016-5571-y.

(10) Sinditskii VP, Filatov SA, Kolesov VI, Kapranova KO, Asachenkob AF, Nechaevb MS, et al. Combustion behavior and physico-chemical properties of dihydroxylammonium 5,5′-bistetrazole-1,1′-diolate (TKX-50). Thermochim Acta. 2015;614:85–92. doi: 10.1016/j.tca.2015.06.019.

(11) Xu X, Chen D, Li H, Yan M, Xiong Y, Zhao H, et al. Crystal structure evolution of an energetic compound dihydroxylammonium 5,5′-bistetrazole-1,1′-diolate induced by solvents. RSC Adv. 2020;10:11939–44. doi: 10.1039/D0RA01182G.

(12) Yuan B, Yu ZJ, Bernstein ER. Initial mechanisms for the decomposition of electronically excited energetic salts: TKX-50 and MAD-X. J Phys Chem A. 2015;119:2965–81. doi: 10.1021/jp510995z.

(13) Yan QL, Zeman S, Sánchez Jiménez PE, Zhao FQ, Pérez-Maqueda LA, Málek J. The effect of polymer matrices on the thermal hazard properties of RDX-based PBXs by using model-free and combined kinetic analysis. J Hazard Mater. 2014;271:185–95. doi: 10.1016/j.jhazmat.2014.02.019.

(14) Yan QL, Zeman S, Elbeih A. Recent advances in thermal analysis and stability evaluation of insensitive plastic bonded explosives (PBXs). Thermochim Acta. 2012;537:1–12. doi: 10.1016/j.tca.2012.03.009.

(15) Jaw KS, Lee JS. Thermal behaviors of PETN base polymer bonded explosives. J Therm Anal Calor. 2008;93:953–7. doi: 10.1007/s10973-006-7736-6.

(16) An Q, Goddard WA, Zybin SV, Luo SN. Inhibition of hotspot formation in polymer bonded explosives using an interface matching low density polymer coating at the polymer–explosive interface. J Phys Chem C. 2014;118:19918–28. doi: 10.1021/jp506501r.

(17) Guo L, Xu H, Wu N, Yuan S, Zhou L, Wang D, et al. Molecular dynamics simulation of the effect of the thermal and mechanical

properties of addition liquid silicone rubber modified by carbon nanotubes with different radii. e-Polymers. 2023;23:20228105. doi: 10.1515/epoly-2022-8105.
(18) Lv YL, Ruan CL. Molecular dynamics simulation of nonisothermal crystallization of a single polyethylene chain and short polyethylene chains based on OPLS force field. e-Polymers. 2022;22:136–46. doi: 10.1515/epoly-2022-0019.
(19) Dong G, Liu HZ, Deng L, Yu HY, Zhou X, Tang XQ, et al. Study on the interfacial interaction between ammonium perchlorate and hydroxyl-terminated polybutadiene in solid propellants by molecular dynamics simulation. e-Polymers. 2022;22:264–75. doi: 10.1515/epoly-2022-0016.
(20) Rice JR. Elastic-plastic fracture mechanics. Eng Fract Mech. 1973;5:1019–22. doi: 10.1016/0013-7944(73)90068-4.
(21) Theodorou DN, Boone TD, Dodd LR, Mansfield KF. Stress tensor in model polymer systems with periodic boundaries. Macromol Theory Simul. 1993;2:191–238. doi: 10.1002/mats.1993.040020204.
(22) Swenson RJ. Comments on virial theorems for bounded systems. Am J Phys. 1983;51:940–2. doi: 10.1119/1.13390.
(23) Ma XF, Xiao JJ, Yin KL, Xiao HM. Molecular dynamics simulation on mechanical properties of TATB/PCTFE composite material. Chin J Chem Phys. 2005;18:55–8. doi: 10.1088/1674-0068/18/1/55-58.
(24) Xiao JJ, Gu CG, Fang GY, Zhu W, Xiao HM. Theoretical study on binding energies and mechanical properties of TATB-based PBX. Acta Chim Sin. 2005;63(6):439–44. doi: 10.3321/j.issn:0567-7351.2005.06.001.
(25) Stevens LL, Eckhardt CJ. The elastic constants and related properties of B-HMX determined by Brillouin scattering. J Chem Phys. 2005;122:174701–8. doi: 10.1063/1.1883627.
(26) Talawar MB, Agarwal AP, Anniyappan M, Gore GM, Asthana SN, Venugopalan S. Method for preparation of fine TATB (2–5 μm) and its evaluation in plastic bonded explosive (PBX) formulations. J Hazard Mater. 2006;137:1848–52. doi: 10.1016/j.jhazmat.2006.05.031.
(27) Han Z, Wang BL. A new method for predicting detonation velocity of composite explosive. Explos Shock Waves. 2014;34:421–6. doi: 10.11883/1001-1455(2014)04-0421-06.
(28) Chen L, Lu JY, Feng CG. Experimental and theoretical investigation on laser supported detonation waves in air. Chin J High Pressure Phys. 2010;24:154–60. doi: 10.3724/SP.J.1187.2010.00969.
(29) Yu YH, Chen SS, Li X, Zhu JP, Liang H, Shu QH. Molecular dynamics simulations for 5,5′-bistetrazole-1,1′-diolate (TKX-50) and its PBXs. RSC Adv. 2016;6:20034–41. doi: 10.1039/C5RA27912G.